

Electron Enhanced Growth of Crystalline Gallium Nitride Thin Films at Room Temperature and 100 °C Using Sequential Surface Reactions

Jaclyn K. Sprenger,[†] Andrew S. Cavanagh,[†] Huaxing Sun,[†] Kathryn J. Wahl,[‡] Alexana Roshko,[§] and Steven M. George^{†,||}

[†]Department of Chemistry and Biochemistry, University of Colorado, Boulder, Colorado 80309, United States

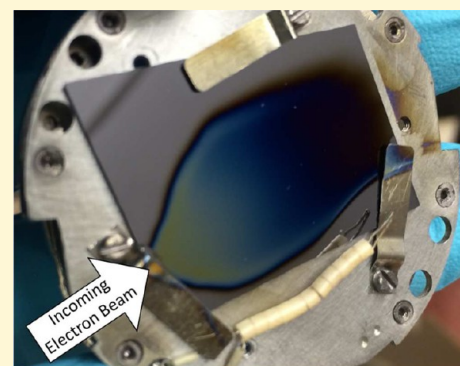
[‡]Chemistry Division, Naval Research Laboratory, Washington, DC 20375, United States

[§]National Institute of Standards and Technology, Boulder, Colorado 80305, United States

^{||}Department of Mechanical Engineering, University of Colorado, Boulder, Colorado 80309, United States

ABSTRACT: Low energy electrons may provide mechanisms to enhance thin film growth at low temperatures. As a proof of concept, this work demonstrated the deposition of gallium nitride (GaN) films over areas of ~ 5 cm² at room temperature and 100 °C using electrons with a low energy of 50 eV from an electron flood gun. The GaN films were deposited on Si(111) wafers using a cycle of reactions similar to the sequence employed for GaN atomic layer deposition (ALD). Trimethylgallium (Ga(CH₃)₃, TMG), hydrogen (H) radicals and ammonia (NH₃) were employed as the reactants with electron exposures included in the reaction cycle after the TMG/H and NH₃ exposures. A number of *ex situ* techniques were then employed to analyze the GaN films. Spectroscopic ellipsometry measurements revealed that the GaN films grew linearly with the number of reaction cycles. Linear growth rates of up to 1.3 Å/cycle were obtained from the surface areas receiving the highest electron fluxes.

Grazing incidence X-ray diffraction analysis revealed polycrystalline GaN films with the wurtzite crystal structure. Transmission electron microscopy (TEM) images showed crystalline grains with diameters between 2 and 10 nm depending on the growth temperature. X-ray photoelectron spectroscopy depth-profiling displayed no oxygen contamination when the GaN films were capped with Al prior to atmospheric exposure. However, the carbon concentrations in the GaN films were 10–35 at. %. The mechanism for the low temperature GaN growth is believed to result from the electron stimulated desorption (ESD) of hydrogen. Hydrogen ESD yields dangling bonds that facilitate Ga–N bond formation. Mass spectrometry measurements performed concurrently with the reaction cycles revealed increases in the pressure of H₂ and various GaN etch products during the electron beam exposures. The amount of H₂ and GaN etch products increased with electron beam energy from 25 to 200 eV. These results indicate that the GaN growth occurs with competing GaN etching during the reaction cycles.



1. INTRODUCTION

Gallium nitride (GaN) is an important wide band gap semiconductor that has many applications in optoelectronics^{1,2} and high power electronics.^{3,4} However, bulk GaN single crystals are not easily produced using conventional methods.⁵ GaN devices rely on GaN heteroepitaxy on other substrates.⁶ This situation increases the importance of depositing GaN using vapor phase processes such as metalorganic chemical vapor deposition^{6–8} (MOCVD), hydride vapor phase epitaxy⁹ (HVPE), and molecular beam epitaxy¹⁰ (MBE) techniques. Unfortunately, these vapor phase processes require high temperatures. For example, temperatures of 800–1100 °C are needed for GaN growth using MOCVD with trimethylgallium (TMG) or triethylgallium (TEG) and NH₃.^{6–8} These high temperatures preclude GaN deposition on many thermally sensitive substrates and device structures. One goal of this work was to develop a method to lower the temperature of GaN thin film growth.

Another goal of this work was to define a GaN atomic layer deposition (ALD) process at low temperatures using sequential, self-limiting surface reactions. ALD techniques are able to deposit thin films conformally with atomic layer control.¹¹ The sequential surface reactions utilized for GaN ALD also allow for the addition of nonthermal enhancement between or during the sequential reactions. Thermal GaN ALD was initially reported using either TMG or TEG and NH₃ as the reactants at temperature ranging from 450 to 900 °C.^{12–14} The use of a hot filament to decompose the NH₃ also produced GaN ALD films at 250–350 °C using TEG and NH₃.¹⁵ GaCl and NH₃ were used as the reactants for GaN ALD at temperatures from 350 to 400 °C.^{16,17} Slightly higher temperatures of 500–750 °C were required for GaN ALD

Received: February 16, 2016

Revised: June 22, 2016

Published: July 1, 2016

using GaCl₃ and NH₃.^{18,19} TMG and a NH₃ plasma has also been used for GaN ALD at temperatures from 185 to 385 °C.^{20,21} In this work, TMG, hydrogen (H) radicals and NH₃ were employed as the reactants with electron exposures included in the reaction sequence after the TMG/H and NH₃ exposures to lower the required temperatures for GaN ALD. TMG was employed instead of TEG because of its higher vapor pressure.

The electron exposures were used for nonthermal enhancement of GaN ALD by electron stimulated desorption (ESD).^{22,23} ESD can be used to desorb a variety of surface species, such as hydrogen and halogens, from surfaces.^{22,23} In particular, the ESD of hydrogen from GaN is an efficient process.^{24,25} Earlier studies have reported an ESD cross section for hydrogen from GaN(0001) of 2×10^{-17} cm² at 90 eV.²⁴ This ESD cross section is much higher than previously reported ESD cross sections for hydrogen from Si(100).^{26–30} ESD can occur via the Menzel–Gomer–Redhead^{31,32} (MGR) or Knotek–Feibelman^{33,34} (KF) mechanisms. The ESD of hydrogen will create free dangling bond sites on the surface. These dangling bond sites can be created at temperatures much lower than 250–500 °C where hydrogen desorbs thermally from GaN surfaces.^{35–37} The dangling bond sites are expected to promote bond formation with other reactants with little or no activation barrier to facilitate thin film growth at low temperatures.

A similar ESD approach has been pursued for nanoscale patterning on silicon surfaces.³⁸ This work is based on the ability of electrons from the scanning tunneling microscope (STM) to desorb hydrogen by ESD from silicon surfaces.^{28,30,38,39} Hydrogen is observed to desorb from Si(100)-2 × 1 surfaces and leave behind silicon dangling bonds.^{28,30,38,40} The reactive dangling bonds can adsorb other reactants such as Al, Fe(CO)₅ or O₂.^{26,41,42} The remaining hydrogen serves as a mask to prevent adsorption. Hydrogen ESD has been employed to form Al,⁴² Fe⁴³ and oxide⁴¹ nanoscale patterns on Si(100) surfaces. In contrast, the approach in this paper uses ESD after sequential TMG/H and NH₃ reactant exposures to grow GaN thin films. This procedure also uses an electron flood gun for hydrogen ESD over surface areas of ~5 cm².

The proposed stepwise sequence of the surface reactions for low temperature GaN growth is shown in Figure 1. A hydrogen atom exposure after the TMG exposure is intended to replace the –CH₃ groups with hydrogen. Electron beam exposures at 50 eV after the TMG/H and NH₃ exposures are expected to desorb hydrogen and form dangling bonds on the GaN surface. Using this proposed stepwise sequence of reactions, GaN film growth on Si(111) wafers was conducted at room temperature and 100 °C. Because of the high reactivity of the dangling bonds, the GaN film growth was performed in an ultrahigh vacuum (UHV) chamber to minimize competitive adsorption from other reactants such as H₂O. Mass spectrometry was also employed to analyze the gas species resulting from the ESD during the reaction sequence.

The GaN films were then analyzed using a variety of *ex situ* techniques. The thickness of these GaN films were measured using spectroscopic ellipsometry (SE). The crystallinity of the GaN films was characterized using grazing incidence X-ray diffraction (GIXRD). The size of the crystallites in the GaN films was established using high resolution transmission microscopy (HRTEM). The composition of the GaN films was measured using X-ray photoelectron spectroscopy (XPS).

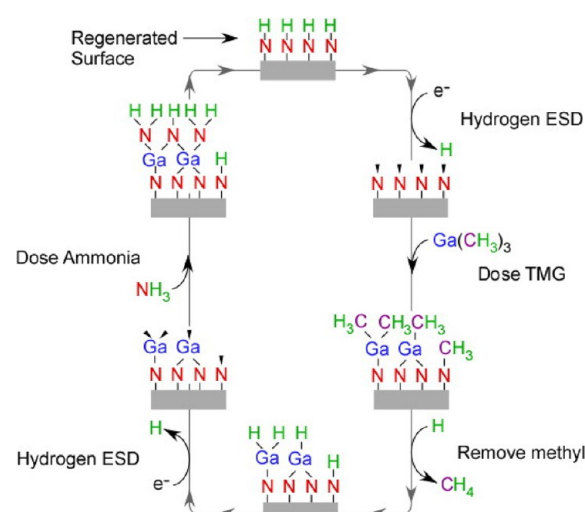


Figure 1. Proposed growth mechanism for electron-enhanced GaN growth using sequential surface reactions.

These analysis techniques can reveal if low temperature growth of crystalline GaN films is possible using electron enhancement at low electron energies of 50 eV.

2. EXPERIMENTAL SECTION

2.1. Vacuum Chamber. The low temperature GaN film growth was conducted in an UHV chamber that was attached to a load lock chamber. Figure 2 shows a schematic of the UHV chamber and the

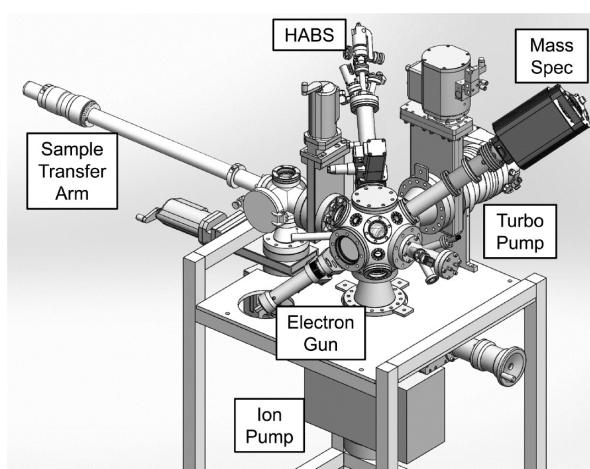


Figure 2. Experimental schematic of vacuum apparatus.

load lock. The core of this UHV chamber is a 4.5" spherical cube (Kimball Physics Inc.). A magnetic sample transfer arm (Thermionics) is attached to the load lock chamber. A gate valve separates the load lock and main chamber. The chamber was pumped with a turbomolecular pump (HiPace 300C, 260 L/s for N₂, Pfeiffer Vacuum Technology AG) during the reaction cycles and additionally with an ion pump (TiTan 100L Variable Element, 100 L/s, Gamma Vacuum) between experiments.

The sample stage (Thermionics) was heated using a temperature-regulated filament. This filament was controlled using a LabVIEW-based proportional-integral-derivative (PID) control. Without heating, the temperature of the sample stage was at room temperature. With the filament heating, the sample stage could be raised to 400 °C. The sample stage included three compression clips that secured the Si(111) wafers and a thermocouple to measure the temperature. The sample stage was grounded to prevent charge build-up.

A beam of low energy electrons was produced using an electron flood gun with a yttria-coated iridium filament (Model EGA-1012, Kimball Physics Inc.). The electron flood gun could produce electron energies from 5 to 1000 eV at electron currents from 1 to 2000 μA . Electrons from the electron gun were incident on the Si(111) substrate at 55° from the surface normal. The distance between the end of the electron gun and the Si(111) substrate was approximately 2.5 cm. Each electron beam exposure was conducted for ~ 120 s. The chamber pressure during the electron exposures was $\leq 1 \times 10^{-7}$ Torr.

Precursors were introduced into the UHV chamber through miniature microdispensing pulse valves (Parker Hannifin Corp.). Prior to introduction, the NH_3 and H_2 lines were passed through hydride and hydrogen gas purifiers (Entegris Inc.), respectively. The valves were open for 100 ms to dose the TMG and NH_3 precursors. The pressure transients in the vacuum chamber during the TMG and NH_3 exposures were each ~ 1 mTorr.

A hydrogen atom beam source (HABS) (MBE-Komponenten GmbH) was used to produce the hydrogen radicals. The hydrogen radicals were formed by cracking H_2 using a tungsten capillary at 1900°C . The chamber pressure during the hydrogen atom beam exposure was $\sim 1 \times 10^{-5}$ Torr with ~ 1 sccm of H_2 flowing through the HABS. The working distance from the end of tungsten capillary in the HABS to the Si(111) substrate was ~ 20 cm. The hydrogen radical flux was incident on the Si(111) substrate at an angle of 55° from surface normal. The HABS was expected to have a flux of $(1-5) \times 10^{15}$ H atoms $\text{cm}^{-2} \text{s}^{-1}$ based on the operating conditions. Hydrogen radical exposures covered a surface area of ~ 5 cm^2 . The hydrogen atom exposure time was typically 100 s. Shorter hydrogen atom exposure times led to more carbon incorporation in the GaN films.

The UHV chamber also was equipped with a mass spectrometer (PrismaPlus QMG 220 M with C-SEM detector, Pfeiffer Vacuum Inc.). This mass spectrometer could measure mass signals up to $m/z = 200$ amu. This mass spectrometer also has an internal ion current-to-pressure calibration that allows partial pressures to be estimated from ion currents. The mass spectrometer is located in the top right-hand side of Figure 2. The HABS is positioned just left of center in the top portion of Figure 2. The electron gun is shown in Figure 2 in the front lower left of the UHV chamber. A z-translation stage allowed the electron flood gun to be extended and retracted to accommodate the sample transfer arm. The ion pump is located underneath the main UHV chamber. The turbomolecular pump is positioned in back of the UHV chamber on the right-hand side behind the mass spectrometer.

After the completion of most of the work presented in this paper, an *in situ* ellipsometer (Film Sense, FS-1 Multi-Wavelength Ellipsometer) was installed on the chamber. This *in situ* ellipsometer provided a method to study the effect of reaction parameters on the growth rate of the GaN film. In addition, the experimental apparatus was also upgraded to include a small second chamber where the sample could be analyzed using Auger electron spectroscopy using a cylindrical mirror analyzer (RBD Instruments, microCMA Compact Auger Analyzer). This Auger analysis chamber was separated from the main chamber by a gate valve. The sample could be moved between the main chamber and the Auger analysis chamber using a magnetic transfer mechanism.

2.2. Chemicals and Materials. GaN films were grown using trimethylgallium ($\text{Ga}(\text{CH}_3)_3$; 99.9999%, electronics grade, Strem), ammonia (NH_3 ; 99.999%, anhydrous, Airgas) and hydrogen (H_2 ; research grade, Airgas). Films were deposited on boron-doped Si(111) substrates (Silicon Valley Microelectronics, Inc.). The substrates were rinsed with acetone and methanol, and cleaned with Nano-Strip (Cyantec Corporation). The silicon native oxide was removed and the surface was hydrogen-passivated using dilute hydrofluoric (HF) acid (50:1 $\text{H}_2\text{O}:\text{HF}$).

The silicon substrate on the sample stage was loaded into the load lock chamber and the background pressure was reduced to 1×10^{-6} Torr. The silicon substrate on the sample stage and the surrounding load lock chamber were then UV-irradiated for 1 h using UV lamps (RBD Instruments) to desorb water and other surface species from the silicon substrate and chamber walls.⁴⁴ After the pressure in the load lock was reduced to approximately 1×10^{-8} Torr, the silicon substrate

on the sample stage was transferred into the main chamber. The silicon substrate on the sample holder and the main chamber were again irradiated with UV light for 1 h. Prior to deposition, the Si(111) wafer was also cleaned using a 100 s hydrogen atom beam exposure at a flux of $(1-5) \times 10^{15}$ H atoms $\text{cm}^{-2} \text{s}^{-1}$.

For comparison, GaN films were also deposited on the Ga-face of single-crystal GaN(0001) substrates (Kyma Technologies) provided by the Naval Research Laboratory. The Ga-face was employed because the previous studies of hydrogen ESD on GaN substrates were performed on the Ga-face of GaN(0001).⁴⁵ The GaN(0001) substrates were N+ (Si doped) with a maximum off-cut of 0.33 degrees. To clean the single-crystal GaN wafers, the samples were dipped in dilute HF (50:1 $\text{H}_2\text{O}:\text{HF}$) for 5 min at 27°C , rinsed with deionized water, dipped in Nanostrip at 80°C for 10 min, rinsed again with deionized water, and then blown dry with nitrogen.⁴⁶ The GaN wafers were then attached to a Si(111) wafer using 9 mm diameter carbon adhesive tape (SPI Supplies). After transfer to the vacuum chamber, the sample was further cleaned with 30 cycles of the following reaction sequence: 5 s TMG exposure; 5 s purge; 30 s HABS exposure; 5 s purge; and a 300 s HABS exposure. These conditions were close to previous *in situ* cleaning procedures reported for GaN samples.⁴⁶

2.3. Ex situ Film Analysis. The GaN films were analyzed using a variety of *ex situ* techniques. The film thickness, index of refraction, n , and extinction coefficient, k , were determined using a spectroscopic ellipsometer (Model M-2000, J.A. Woollam Co., Inc.). The SE data was fitted with a Tauc-Lorentz model using the CompleteEASE software package (J.A. Woollam Co., Inc.) to obtain the film thickness and optical properties.

The crystallinity of the GaN films was determined using grazing incidence X-ray diffraction (GIXRD) at the Naval Research Laboratory. The diffraction patterns were obtained with an X-ray diffractometer (SmartLab System, Rigaku) using $\text{Cu K}\alpha$ irradiation at an incident angle of 0.3° . The diameter of the GaN crystallites was estimated based on the width of the diffraction peaks using the Scherrer formula.⁴⁷

The TEM images of the GaN films were recorded at the National Institute of Science and Technology in Boulder (NIST-Boulder). The cross-sectional samples for TEM were prepared by focused ion beam (FIB) Ga milling (Auriga Dual Beam FIB, Carl Zeiss)⁴⁸ after deposition of a protective platinum layer. Low-energy Ar ion milling at 850 eV was used to remove the FIB-induced surface damage. The samples were imaged at 200 kV in a high resolution transmission electron microscopy (HRTEM) instrument (JEM-ARM200F TEM, JEOL).⁴⁸ This HRTEM contained an aberration-corrected probe for scanning transmission electron microscopy (STEM).

The film composition was determined by X-ray photoelectron spectroscopy (XPS) analysis using an X-ray photoelectron spectrometer (PHI 5600) at the University of Colorado. The spectrometer used a monochromatic Al $\text{K}\alpha$ source at 1486.6 eV. The pass energy was 29.35 eV and the step size was 0.25 eV. An electron beam neutralizer was used during the XPS measurements. XPS depth-profiling and surface carbon removal were conducted using argon ion sputtering. The XPS data was collected using AugerScan (RBD Instruments). The XPS data was analyzed in CasaXPS (Casa Software Ltd.).

3. RESULTS AND DISCUSSION

3.1. Film Growth and Characterization Using Spectroscopic Ellipsometry. The GaN films were grown at room temperature (27°C) and 100°C using the stepwise sequence of exposures shown in Figure 1. The exact reaction sequence was: TMG pressure transient of ~ 1 mTorr; purge of 15 s; HABS exposure of 100 s; purge of 90 s; electron exposure of 120 s; NH_3 pressure transient of ~ 1 mTorr; purge of 90 s; and electron exposure of 120 s. The electron energy was 50 eV and the electron emission current from the filament was 150 μA . The electron current incident on the sample during the electron exposures was $\sim 75 \mu\text{A}$ for 120 s.

Figure 3 shows a photo of a GaN film on a Si(111) wafer after 600 reaction cycles at 27 °C. The GaN film was clearly

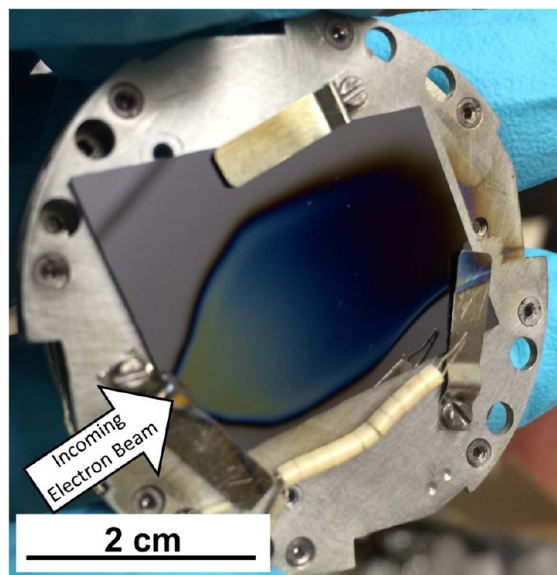


Figure 3. Photo of GaN film grown on Si(111) substrate at 27 °C.

visible on the Si(111) wafer and appeared as a gradient of colors ranging from light blue to dark brown. This GaN film has dimensions of ~ 3.0 cm \times 1.5 cm. The vacuum chamber background pressure before the 600 cycles was 5×10^{-9} Torr. During the purge portion of the reaction sequence, the background pressure increased to $\sim 2 \times 10^{-8}$ Torr during the 600 cycles.

After the GaN film growth, *ex situ* spectroscopic ellipsometry was used to measure the film thickness on the Si(111) wafer. Film thicknesses varied across the Si(111) wafer from 80 nm close to the electron gun to 30 nm away from the electron gun. This range of film thicknesses is attributed to the varying electron beam flux across the surface. The electron gun emits electrons in a Gaussian spatial distribution. The incident electron flux was 55° from the surface normal of the Si(111) wafer. The electron beam also is diverging because of space-charge effects that are more severe at low electron energies. These factors cause the electron beam diameter to increase with propagation distance from the electron gun.

The electrons impacting the far side of the Si(111) wafer travel approximately twice the distance from the electron gun source as electron impacting the near side of the Si(111) wafer. More uniform film thicknesses would be obtained with incident electron fluxes that are normal to the surface. However, these incident electron fluxes from the electron gun would still have a Gaussian spatial distribution. Electron fluxes that are even more uniform could also be obtained by extracting electrons from the positive column of a DC glow discharge plasma.⁴⁹

To determine GaN film growth rates on the Si(111) wafer, the film thicknesses were measured using spectroscopic ellipsometry at various positions along the gradient as shown in Figure 4a. Thickness measurements were performed after 150, 250, 300, 400, and 600 reaction cycles and are summarized in Figure 4b. Figure 4b reveals that there is a linear increase in film thickness versus number of reaction cycles. The slight deviations from linearity for the thicknesses after 250 and 400 cycles may be caused by the difficulty in manually replicating

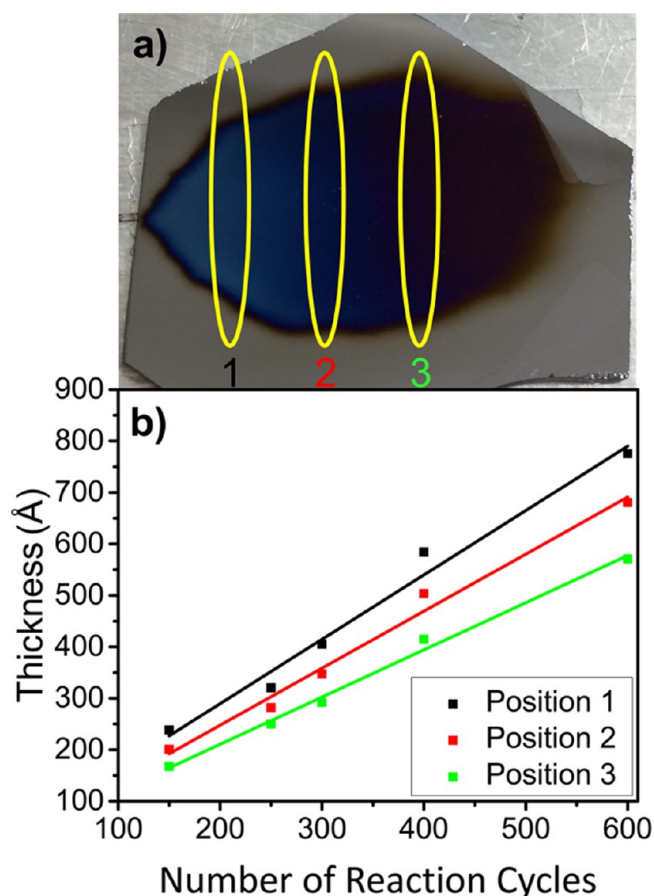


Figure 4. (a) GaN film on Si(111) wafer showing three positions for analysis using spectroscopic ellipsometry. (b) Thickness of GaN versus number of reaction cycles at the three positions.

the same locations on the various samples. The growth rate varied from 0.9 to 1.3 Å/cycle across the three positions shown in Figure 4a. Slightly smaller GaN growth rates were also observed at 100 °C.

The measured GaN growth rates from 0.9 to 1.3 Å/cycle at room temperature are postulated to be obtained under self-limiting reactant exposures. Additional *in situ* ellipsometry measurements performed after the completion of the experimental results displayed in Figure 4 revealed that the ~ 1 mTorr pressure transients for the reactants were sufficient for the surface reactions to reach completion. In contrast, the GaN growth rate dependence on electron exposure time was not self-limiting. The *in situ* ellipsometer experiments have revealed that the GaN growth rate increases for longer electron exposure times. The rate of increase does begin to level off for electron exposure times >60 s. However, the GaN growth rate is still increasing for electron exposure times as long as 250 s. This behavior is consistent with only a small loss of hydrogen coverage resulting from hydrogen ESD as discussed later in Section 3.6.

The GaN growth rates from 0.9 to 1.3 Å/cycle are somewhat smaller than the previous GaN growth rates reported by thermal GaN ALD. Thermal ALD experiments using TEG and NH_3 as the reactants obtained GaN growth rates of ~ 1.9 Å/cycle.¹⁴ Other thermal ALD investigations using GaCl_3 and NH_3 as the reactants have measured growth rates of ~ 2 Å/cycle¹⁸ and ~ 3 Å/cycle.¹⁹ Additional thermal ALD studies using GaCl and NH_3 as the reactants have obtained growth

rates of ~ 2.5 Å/cycle.^{16,17} However, plasma ALD studies using TMG and NH_3 as the reactants have reported smaller GaN growth rates of ~ 0.22 Å/cycle²¹ and ~ 0.51 Å/cycle.²⁰

Control experiments were performed to understand the growth mechanism. The first control experiment replaced the electron gun exposures at 50 eV after the TMG/H and NH_3 exposures with an equivalent length purge for 300 cycles. All other conditions remained the same as described for the growth of the GaN film shown in Figure 3. Subsequently, *ex situ* spectroscopic ellipsometry and XPS measurements observed no film growth.

Experiments were also performed by removing the precursor doses while maintaining all other reaction conditions for 300 cycles. No film growth was observed by *ex situ* spectroscopic ellipsometry measurements without the TMG doses. Likewise, the reactions performed without NH_3 doses showed no film growth. Control experiments were also performed without HABS exposures. All other reaction conditions were maintained and a 100 s purge replaced the HABS exposure. *Ex situ* spectroscopic ellipsometry measurements observed film growth with a growth rate consistent with the growth rates obtained using the HABS exposures. However, *ex situ* XPS analysis revealed a carbon contamination of 27 at. % for GaN films grown at 27 °C.

Spectroscopic ellipsometry was used to characterize the optical properties of the GaN films. Figure 5 shows the index of

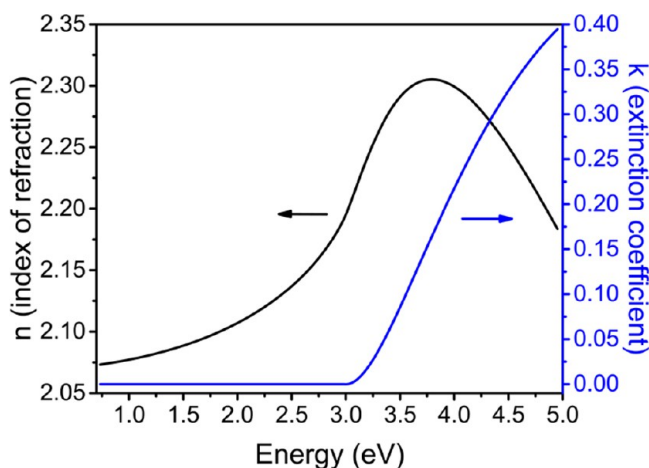


Figure 5. Index of refraction, n , and extinction coefficient, k , versus radiation energy for the GaN film on Si(111) wafer.

refraction, n , and the extinction coefficient, k , of the GaN films grown on the Si(111) wafers. The extinction coefficients indicate that the GaN films begin to absorb radiation at energies slightly greater than 3 eV. This absorption threshold is consistent with the bandgap for bulk GaN of 3.4 eV.^{3,12} In addition, the index of refraction of the GaN films is $n = 2.07$ at 1.0 eV and reaches a peak value of approximately $n = 2.3$ at energies above the bandgap energy. These results are slightly smaller than the values of $n = 2.33$ at 1.0 eV and $n = 2.67$ at 3.38 eV reported in the literature.⁵⁰ The smaller refractive indices may result from the high carbon concentration in the polycrystalline GaN films.

3.2. Crystallinity from GIXRD Measurements. The crystallinity of the GaN films was established using grazing incidence X-ray diffraction (GIXRD) and transmission electron microscopy (TEM). GIXRD results for the GaN films grown

on Si(111) wafers are shown in Figure 6. Figure 6a shows the results for a GaN film grown at 27 °C using 807 reaction cycles.

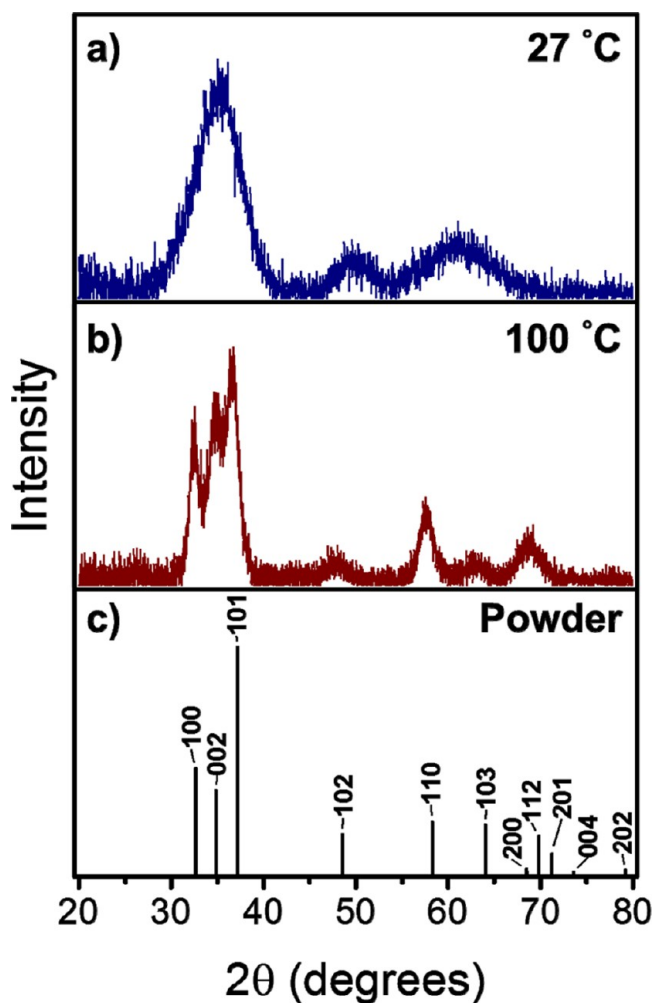


Figure 6. GIXRD of GaN films grown on Si(111) wafers at (a) 27 °C and (b) 100 °C. (c) Positions and intensities of diffraction peaks for crystalline wurtzite GaN powder.

This film had a thickness of ~ 1200 Å at position 1 as defined in Figure 4. Figure 6b displays the results for a GaN film grown at 100 °C using 827 reaction cycles. This film had a thickness of ~ 600 Å at position 1 as defined in Figure 4. For comparison, the XRD results for a crystalline wurtzite GaN powder are shown in Figure 6c.^{51,52} The Miller indices are associated with each peak and the length of the lines indicates the relative intensities.

A comparison between Figure 6b and 6c indicates that the strong 100, 002, and 101 diffraction peaks of crystalline wurtzite GaN are clearly observed in the GaN film grown at 100 °C. All of the other lower intensity peaks for crystalline wurtzite GaN are also present in the GaN film grown at 100 °C. The major difference is that the peaks in Figure 6b are broadened relative to the peaks for crystalline GaN powder.⁵³ This broadening is consistent with a fine-grained, polycrystalline GaN film grown at 100 °C. The size of the GaN crystallites in the GaN film grown at 100 °C was estimated from the width of the diffraction peaks using the Scherrer equation. This estimate yields GaN crystallites with a diameter of 5–7 nm.

The diffraction peaks in Figure 6a for the GaN films grown at 27 °C are broader than the diffraction peaks for the GaN films grown at 100 °C in Figure 6b. The broadening leads to a coalescence of the strong 100, 002, and 101 diffraction peaks of crystalline wurtzite GaN into one broad peak. The lower intensity peaks are also broader and are slightly shifted relative to the diffraction peaks of crystalline wurtzite GaN powder. This increased broadening suggests that the polycrystalline grain size is smaller for the GaN films grown at 27 °C. The diameter of the GaN crystallites in the GaN film grown at 27 °C was estimated to be 2–5 nm based on the width of the diffraction peaks using the Scherrer equation.

For comparison, GaN films were also grown on the Ga-face of single-crystal GaN(0001) wafers at 27 and 100 °C to determine if the GaN films would grow epitaxially on a crystalline GaN substrate. Figure 7 shows a picture of a GaN

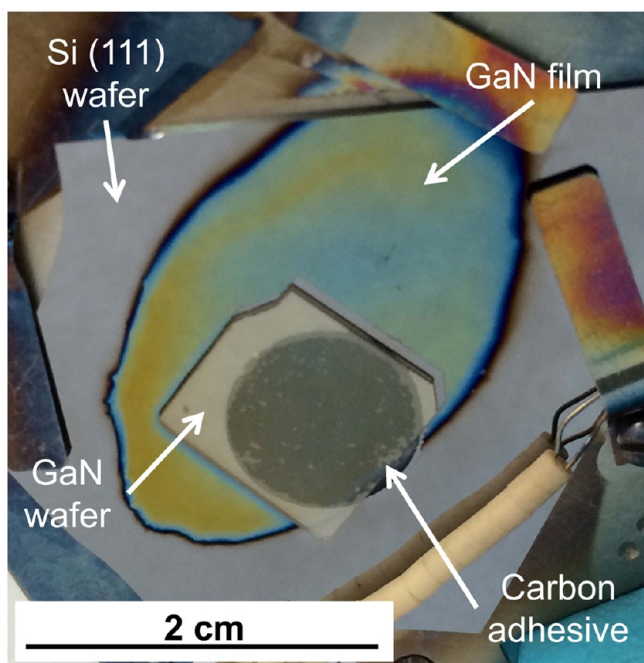


Figure 7. Photo of GaN film grown at 27 °C on a single-crystal GaN(0001) substrate attached to a Si(111) wafer using a carbon adhesive.

film grown on a single-crystal GaN(0001) wafer on a Si(111) wafer after 500 reaction cycles at 27 °C following the same procedure as employed for the GaN film shown in Figure 3. A GaN film is again observed on the Si(111) wafer in agreement with Figure 3. A GaN film is not visible on the single-crystal GaN(0001) wafer because the optical characteristics of the deposited GaN film are nearly identical to the underlying single-crystal GaN(0001) wafer.

The GaN films grown on the Ga-face of single-crystal GaN(0001) wafers were also analyzed using *ex situ* GIXRD measurements performed at the Naval Research Laboratory. The GIXRD measurements showed broad diffraction peaks centered at $\sim 36^\circ$ and $\sim 62^\circ$. In addition, sharp diffraction peaks were also observed as expected from the underlying single-crystal GaN substrate. These results were consistent with a polycrystalline GaN film on the GaN(0001) single-crystal substrate with no evidence for homoepitaxial growth. The results at 27 and 100 °C were similar although the diffraction peaks were broader for the GaN films grown at 27 °C.

3.3. Crystallinity from TEM Measurements. The crystallinity of the deposited GaN films was also verified by TEM imaging. Figure 8a shows a cross-sectional TEM image of

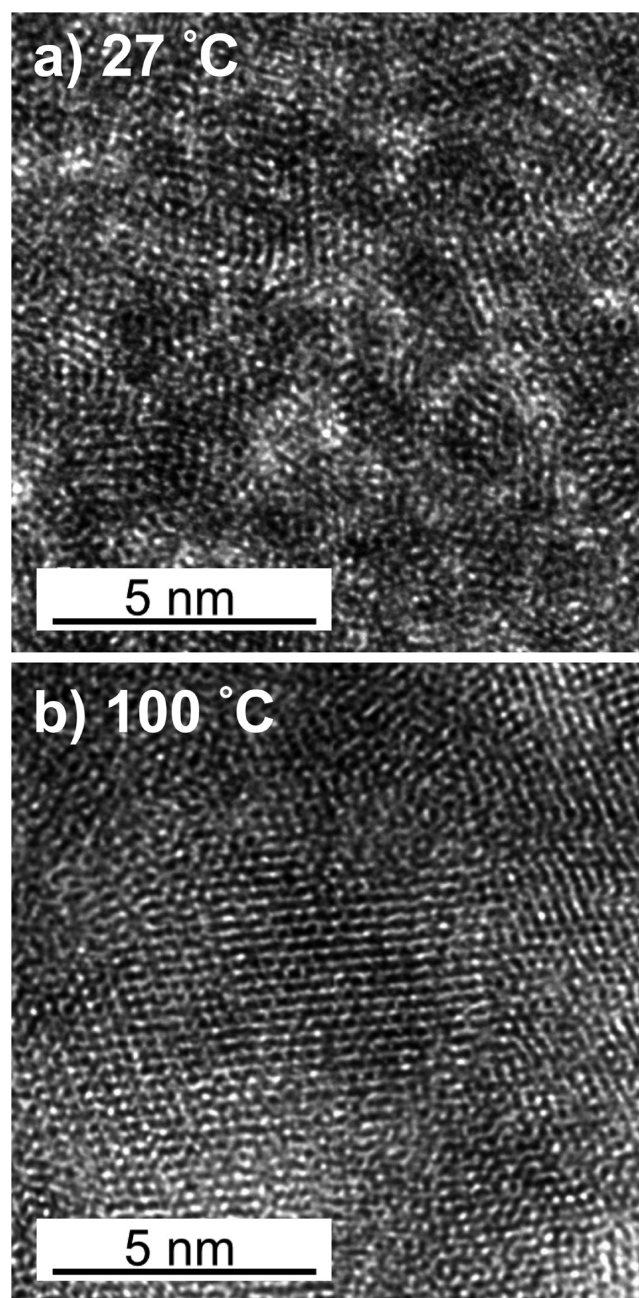


Figure 8. Cross-sectional HRTEM phase contrast images of GaN films grown on Si(111) wafer at (a) 27 °C and (b) 100 °C.

a GaN film grown at 27 °C on a Si(111) wafer using 600 reaction cycles. The crystallites in the GaN films are randomly oriented with no preferred direction. The diameters of the GaN crystallites grown at 27 °C vary from 2 to 5 nm. Crystallinity is also observed in Figure 8b for the GaN films grown at 100 °C on a Si(111) wafer using 600 reaction cycles. The crystallites in the GaN films are again randomly oriented with no preferred direction. However, the diameters of the GaN crystallites grown at 100 °C are larger and vary from 5 to 10 nm. For the GaN films grown at both 27 and 100 °C, the crystallite sizes and

absence of texturing are in excellent agreement with the XRD measurements.

Figure 9 shows high resolution TEM (HRTEM) contrast imaging of a cross section of a GaN film on the Si(111) wafer.

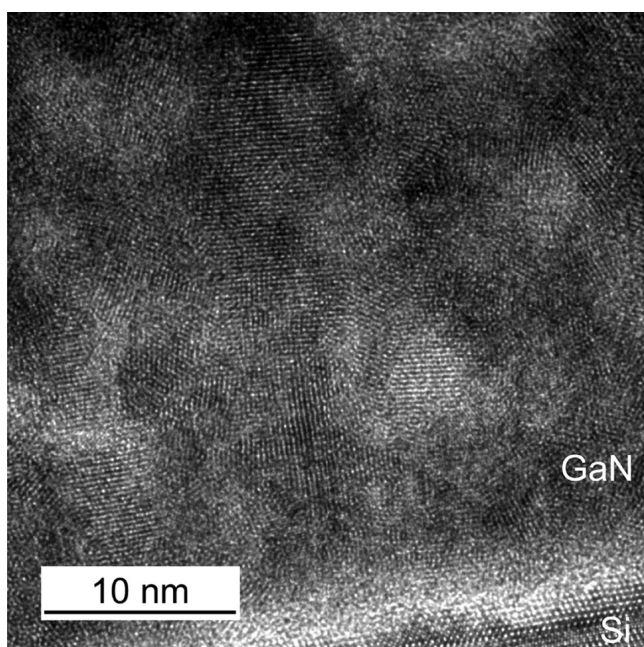


Figure 9. Cross-sectional HRTEM phase contrast image of the GaN film grown on Si(111) wafer at 100 °C.

This GaN film was grown at 100 °C using 630 reaction cycles. The TEM image clearly reveals the presence of crystalline GaN grains with random orientations. The GaN crystallites show no epitaxial growth preference on the Si(111) wafer. The lack of epitaxy may result from the thin amorphous layer with a thickness of ~1 nm at the interface between the Si(111) wafer and the GaN film. This amorphous layer may be attributed to carbon contamination on the initial Si(111) wafer. In agreement with the results in Figure 8b, the GaN crystallites have diameters ranging from 5 to 10 nm.

3.4. Composition from XPS Depth-Profiling Measurements. The cross-sectional composition of the GaN films grown on Si(111) wafers was determined using XPS depth-profiling measurements. Initial XPS depth-profiling measurements revealed that the GaN films oxidized upon exposure to atmosphere. To evaluate the stoichiometry of the GaN films without atmospheric oxidation, an Al capping layer was deposited on the GaN films as a sacrificial oxidant. This Al capping layer was deposited using sequential exposures to trimethylaluminum (TMA) and hydrogen radicals from the HABS.

For the XPS depth-profiling results shown in Figure 10, the Al capping layer was deposited using 575 reaction cycles of TMA and hydrogen radicals at 100 °C. Figure 10 shows that the Al capping layer is oxidized at the surface. This oxidation is attributed to atmospheric exposure. The oxygen profile is consistent with oxygen diffusion into the Al film. The Al capping layer also contains ~20 at. % of nitrogen. This nitrogen is believed to result from the high background pressures of residual NH₃ remaining in the vacuum chamber from the previous GaN growth during the deposition of the Al capping

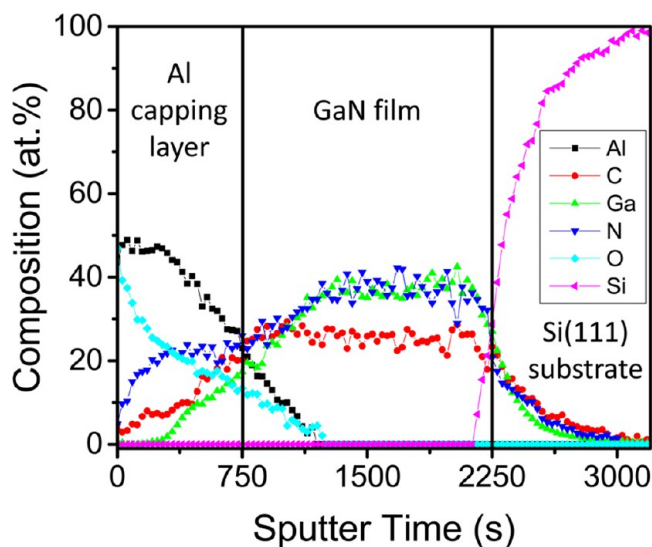


Figure 10. XPS depth profile of GaN film grown on Si(111) wafer showing oxygen-free stoichiometric GaN with some carbon contamination. An Al capping layer protected the GaN film from oxidation.

layer. Al metal films are expected to be reactive with residual NH₃.

Figure 10 also shows the XPS depth-profiling results for the GaN film under the Al capping layer that was grown at 28 °C using 600 reaction cycles. The Al-capped GaN film displays a region of stoichiometric GaN with oxygen levels below the XPS detection limit under the Al cap. However, the GaN film also shows a significant carbon contamination of ~20 at. %. Carbon contamination was present in all the GaN films examined with XPS depth-profiling grown at both 27 and 100 °C. The carbon concentrations were in the range of 12–35 at. % (average: 23 at. %) for the films grown at 27 °C and 10–20 at. % (average: 13 at. %) for the films grown at 100 °C. The carbon concentrations could not be lowered by longer hydrogen radical exposures or higher hydrogen radical fluxes using the HABS.

Carbon contamination is known to be present in GaN grown using either TMG or TEG and the level of carbon contamination increases at lower growth temperatures.⁵⁴ To understand this contamination, many experiments were performed to determine the origin of the carbon in the GaN films. At the end of these GaN film growth studies, an *in situ* Auger spectrometer was added to the vacuum chamber. This Auger spectrometer characterized the carbon on the surface after each step in the reaction cycle. These Auger experiments revealed that the HABS was not removing the carbon after the TMG exposures. In fact, the carbon levels were higher after the HABS exposures. Experiments also revealed that the HABS could not remove the initial carbon on the Si(111) substrate. Carbon concentrations were again larger after the HABS exposures.

The carbon in the GaN films may result from the pyrolysis of residual TMG in the chamber on the hot surfaces of the HABS. TMG pyrolysis in flow tubes⁵⁵ and on hot surfaces⁵⁶ is known to produce methyl radicals. The decomposition of TMG on GaN(0001) during temperature programmed desorption also yields methyl radicals.⁵⁷ Over the course of many GaN growth experiments, TMG pyrolysis may produce a HABS source contaminated with carbon. Subsequent inspection of the HABS

revealed bluish-back discolorations on the HABS surfaces that were consistent with a carbon film buildup over the course of many GaN growth experiments. In addition, residual TMG pressures in the chamber during the HABS step of the reaction sequence may also directly produce methyl radicals.⁵⁶

In spite of the carbon contamination, the GaN films still display crystallinity as shown in Figures 6, 8, and 9. Consequently, the carbon is believed to be present at the grain boundaries between the GaN crystallites. Earlier studies have correlated “yellow” luminescence with carbon in GaN.⁵⁸ Other investigations have observed that the “yellow” luminescence emanates from grain boundaries in GaN.⁵⁹ The carbon could also be substituted for nitrogen or gallium in the GaN crystal or exist in interstitial sites.⁶⁰ However, carbon at the grain boundaries is the more likely possibility. At carbon concentrations as high as 10–20 at. %, the carbon would alter the GaN crystallinity and preclude the agreement between the X-ray diffraction peaks from the GaN film grown at 100 °C and the crystalline wurtzite GaN powder that was observed in Figure 6.

3.5. Mass Spectrometry Measurements of H₂ Desorption and Etch Products. Quadrupole mass spectrometry measurements were performed during the sequential reaction cycles that define GaN film growth on Si(111) wafers. These experiments determined if the electron exposures can desorb enough H₂ and other possible species to be detected by the mass spectrometer. In particular, the mass spectrometer signals from the desorbed H₂ could be used to quantify the ESD and its dependence on electron energy. The presence of other desorbed species generated by the electron exposure may also determine if the electron beam could desorb Ga or N etch species from the growing GaN surface.

The mass spectrometer monitored a variety of species in the gas phase during the electron exposures. These species can be assigned to hydrogen ($m/z = 2$), methyl species ($m/z = 15, 14$), ammonia species ($m/z = 17, 16$), water ($m/z = 18, 17$), gallium isotopes ($m/z = 71, 69$), and gallium hydrides ($m/z = 72, 70$). Figure 11 shows the ion currents for a variety of species during the electron beam exposure following the HABS exposure. The ion currents are ordered relative to the magnitudes of their ion currents.

The electron current from the electron gun starts to increase at ~75 s. The electron current reaches its maximum current at ~100 s. The electron current incident on the sample remains at its maximum current of ~75 μA for 120 s. The ion currents at $m/z = 2$ (H₂⁺) in Figure 11b and $m/z = 69$ (⁶⁹Ga⁺) and $m/z = 70$ (⁶⁹GaH⁺) in Figure 11d increase in conjunction with the electron current. In contrast, the ion currents at $m/z = 18$ (H₂O⁺) in Figure 11d and $m/z = 16$ and 17 (NH₂⁺ and NH₃⁺) in Figure 11a are relatively constant during the increase in electron current. The ion current at $m/z = 15$ (CH₃⁺) in Figure 11c shows only a very small increase with the electron current.

The ion current at $m/z = 2$ (H₂⁺) increases with the electron current and indicates that H₂ is desorbed to produce dangling bond sites. Other species containing gallium such as gallium hydrides at $m/z = 69, 70, 71$, and 72 also increase with the electron current. The $m/z = 69$ species is assigned to ⁶⁹Ga⁺. The $m/z = 70$ species is attributed to ⁶⁹GaH⁺. The $m/z = 71$ species is assigned to either ⁷¹Ga⁺ or ⁶⁹GaH₂⁺. The $m/z = 72$ species is attributed to either ⁶⁹GaH₃⁺ or ⁷¹GaH⁺, respectively. These ion currents are consistent with the existence of gallium hydrides and the etching of the GaN film. These etching products suggest that the observed GaN growth may result

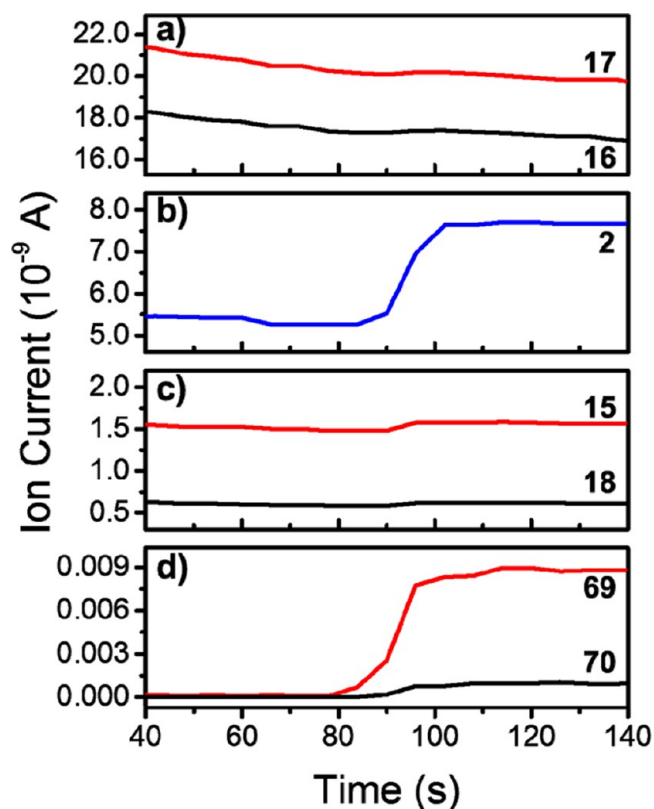


Figure 11. Ion currents for (a) $m/z = 16$ and 17; (b) $m/z = 2$; (c) $m/z = 15$ and 18, and (d) $m/z = 69$ and 70 during the GaN growth on Si(111) wafers after the end of the HABS exposure. The electron current is turned on at ~75 s and reaches its maximum value at ~100 s.

from competing deposition and etching processes. GaN etching with low energy electrons has previously been observed for GaN samples in contact with hydrogen radicals from a H₂ plasma.⁶¹

The pressure changes resulting from the electron exposure were quantified by measuring the ion currents before and during the electron exposures. The H₂ pressure changes during the electron exposures after the TMG/H and NH₃ reactions were nearly identical. The ion current changes at $m/z = 2$ (H₂⁺) versus electron energy are shown in Figure 12a. At each energy, the ion current change increased with electron current from the electron gun and stayed elevated during the 120 s electron exposure. The H₂ pressure prior to the electron exposures was $\sim 2.7 \times 10^{-9}$ Torr using the calibration of the ion current to H₂ pressure of ~ 2 A/Torr. Figure 12a shows that the desorbed H₂ has an electron energy threshold at ~ 25 eV. Pronounced H₂ desorption signals are observed at the electron energy of 50 eV used for GaN film growth. Larger H₂ desorption signals that increase progressively with electron energy are measured at higher electron energies.

The ion current changes for $m/z = 69$ after the TMG/H and NH₃ exposures were also nearly identical and are shown versus electron beam energy in Figure 12b. The gallium hydride species all exhibited a similar dependence on the electron beam energy. The ion current for the gallium hydride species increased with electron current and stayed elevated during the 120 s electron exposure at each electron energy. Figure 12b shows that the desorbed $m/z = 69$ species begins to increase progressively at electron energies >50 eV. Small $m/z = 69$ ion

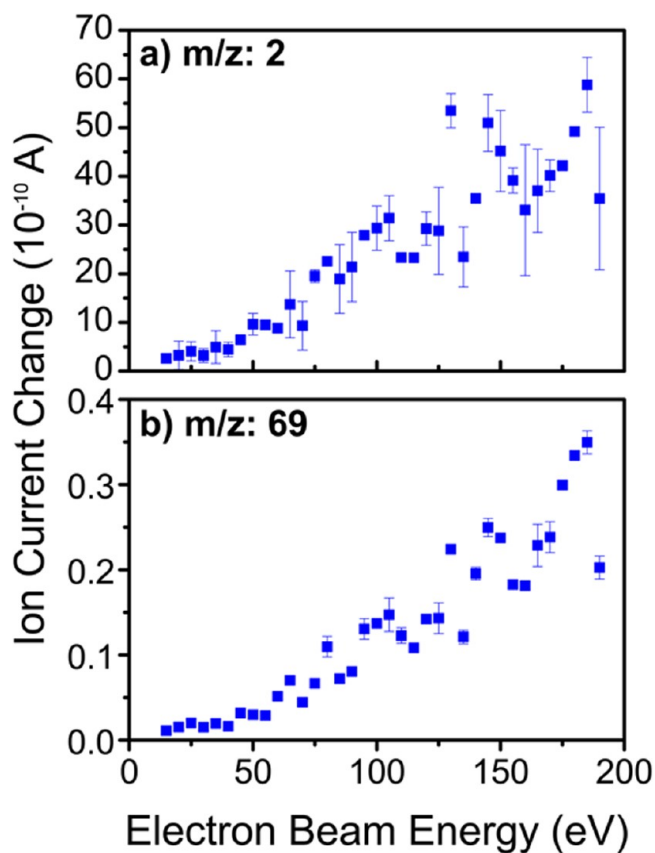


Figure 12. Ion currents for (a) $m/z = 2$ and (b) $m/z = 69$ versus electron beam energy during the electron exposures during GaN growth on Si(111) wafers. The ion currents were nearly identical after the TMG/H and NH_3 reactions.

current changes are observed at the electron energy of 50 eV used for GaN film growth.

A comparison between Figures 12a and 12b can be used to speculate on the optimum electron energy to grow the GaN film. Optimum growth may be related to the ratio between the H_2 ion current change and the gallium hydride ion current change. Higher ratios may predict higher GaN film growth relative to GaN etching. Based on this criteria, electron energies of 50 eV may represent a compromise between reasonable H_2 desorption with minimal desorption of gallium hydride etching products. Additional growth experiments at other electron energies are needed to test this hypothesis.

Other ESD systems also observe an energy threshold and an increase in the desorption yield versus electron energy. For example, a pronounced energy threshold at ~ 24 eV was observed for H desorption from Si(100)-(1 \times 1).^{27,29,62} Energy thresholds are also observed for the ESD of neutral alkalis from alkali halide substrates.⁶³ The thresholds correspond to electron excitation of substrate core levels.⁶³ The energy threshold for Cl^+ ESD from Cl on Si(100) also corresponds to the Cl 3s core level.⁶⁴ The ESD of alkali halide layers from W(110) also shows energy thresholds that are consistent with alkali and halide core levels.⁶⁵

3.6. Constant Ion Currents during Electron Exposures.

Figure 11 shows that the ion currents for $m/z = 2$ (H_2^+) and $m/z = 69$ ($^{69}\text{Ga}^+$) remain constant during the electron beam exposure at 50 eV. The steady ion currents provide no evidence of depletion of the hydrogen coverage over the 120 s electron beam exposure. These constant ion currents suggest that the

electron exposure only removes a small fraction of the hydrogen from a large reservoir of hydrogen on the surface. This explanation can be tested by estimating the amount of hydrogen desorbed based on the electron flux and the hydrogen ESD cross section from GaN.²⁴

The normalized hydrogen coverage, Θ/Θ_0 , will be reduced by hydrogen ESD according to $\Theta/\Theta_0 = \exp[-\sigma D]$.^{27,29} σ is the hydrogen ESD cross section in cm^2 and D is the electron dose in electrons/ cm^2 . The hydrogen ESD cross section is $\sigma = 2 \times 10^{-17} \text{ cm}^2$ at 90 eV.²⁴ This hydrogen ESD cross section at 90 eV will be used as an estimate for the hydrogen ESD cross section at 50 eV. The electron current of $75 \mu\text{A}$ over a surface area of 5 cm^2 yields an electron flux of $\Phi = 9.4 \times 10^{13}$ electrons/ $(\text{cm}^2 \text{ s})$. This flux for a duration of 1 s yields an electron dose of $D = 9.4 \times 10^{13}$ electrons/ cm^2 . The normalized hydrogen coverage after a 1 s electron beam exposure is then determined as $\Theta/\Theta_0 = \exp[-\sigma D] = 0.998$. Approximately 0.2% of the initial hydrogen coverage is desorbed in 1 s. After a 120 s electron beam exposure, the normalized hydrogen coverage remains fairly high and is calculated to be $\Theta/\Theta_0 = 0.80$.

The small predicted changes in the hydrogen coverage may be even smaller if the hydrogen ESD cross section is lower at 50 eV than the hydrogen ESD cross section at 90 eV. A smaller hydrogen ESD cross section at 50 eV would be expected given the results shown in Figure 12a. The small predicted reduction in hydrogen coverage is consistent with the constant $m/z = 2$ (H_2^+) ion current versus electron beam exposure observed in Figure 11b. If there is little change in the hydrogen coverage, then the hydrogen ESD effectively occurs from a constant hydrogen source. The increase in GaN growth rate with increasing electron exposure time is also consistent with the small reduction in hydrogen coverage resulting from hydrogen ESD.

The H_2 pressure change during the electron beam exposure can also be used to estimate the H_2 desorption yield from the surface. Figure 11b shows a change in ion current of $\sim 2 \times 10^{-9}$ A for $m/z = 2$ (H_2^+) during the electron beam exposure. The calibration of the ion current to the H_2 pressure is $\sim 2 \text{ A/Torr}$. Therefore, the ion current change of $\sim 2 \times 10^{-9}$ A represents a H_2 pressure change of $\sim 1 \times 10^{-9}$ Torr. This H_2 pressure change can be converted to a H_2 throughput, Q , using $Q = SP$ where S is the chamber pumping speed and P is the H_2 pressure change. With a H_2 pumping speed of 125 L/s for the turbomolecular pump (HiPace 300C), the throughput is $Q = 4.1 \times 10^{12}$ molecules/s.

Given that the increased throughput from H_2 ESD occurs from a surface area of $\sim 5 \text{ cm}^2$, the H_2 flux from the surface area exposed to the electron beam is $Q/5 = 8.2 \times 10^{11}$ molecules/ $(\text{cm}^2 \text{ s})$. The initial hydrogen coverage is assumed to be $\sim 8.5 \times 10^{14}$ H atoms/ cm^2 based on hydrogen in the (2 \times 2)H structure with three of every four Ga surface atoms bonded to H.⁴⁵ Therefore, the H_2 flux of 8.2×10^{11} molecules/ $(\text{cm}^2 \text{ s})$ represents the desorption of 1.6×10^{12} atoms/ $(\text{cm}^2 \text{ s})$ or only $\sim 0.2\%$ of the initial hydrogen coverage in 1 s. These estimates of hydrogen ESD flux from the H_2 pressure increase during the electron beam exposure in 1 s are in good agreement with the predicted loss of hydrogen coverage in 1 s based on the hydrogen ESD cross sections.

The surface hydrogen coverage could also be repopulated by a reservoir of hydrogen in the underlying GaN film. Hydrogenation of GaN can result from GaN processing steps such as H_2 plasma exposures.^{66,67} For the GaN growth in this study, the hydrogenation of GaN could take place during the

HABS exposure. If the bulk hydrogen diffusion is fast enough, then this hydrogen from the HABS exposure may repopulate the surface hydrogen coverage and help maintain the constant H_2 and gallium hydride desorption during the electron exposure. The hydrogen lost during ESD could also be replenished by the surface diffusion of hydrogen from the surface area surrounding the area exposed to the electron gun. Similar refilling of depleted areas by surface diffusion was the basis of previous laser-induced thermal desorption measurements of surface diffusion.^{68,69}

Another possibility is that the NH_3 background pressure may react with the dangling bonds created by hydrogen ESD during the electron exposures. The ion currents shown in Figure 11a reveal that a large NH_3 background pressure is present during GaN growth. NH_3 adsorption from this NH_3 background pressure would add additional hydrogen to the surface that could be desorbed again through hydrogen ESD. This process would deliver a continuous supply of hydrogen to the surface and also allow nitrogen to be added to the growing GaN film. The actual NH_3 dose would then serve only to replenish the NH_3 background pressure. However, the ion currents for $m/z = 16$ and 17 (NH_3^+ and NH_2^+) in Figure 11a do not show any evidence of a decrease coinciding with the electron exposure. The loss of NH_3 required to refill the dangling bond sites created by hydrogen ESD may be negligible. The slight reduction of the NH_3 background pressure over time in Figure 11a is attributed to slow NH_3 pumping.

If the loss of hydrogen coverage from hydrogen ESD is small or if hydrogen refills the dangling bonds from hydrogen reservoirs or NH_3 adsorption, then the TMG and NH_3 exposures during the sequential reactions would encounter a GaN surface that is largely passivated by hydrogen. TMG may adsorb on the GaN surface through Lewis acid-Lewis base interactions. TMG is a strong Lewis acid.⁷⁰ The nitrogen atoms on the GaN surface have lone pairs that can serve as Lewis bases. At the low temperatures of GaN growth, TMG may be able to adsorb to the surface and remain on the surface until the next electron beam exposure. The electrons may then facilitate the reaction between adsorbed TMG and the NH_3 background pressures. NH_3 may adsorb on dangling bonds and deliver nitrogen during the electron exposures because NH_3 has a high background pressure. NH_3 may also adsorb at Ga surface sites through Lewis acid-Lewis base interactions.

The mass spectrometer results for $m/z = 2$ (H_2^+) in Figure 11b provide a useful measure of the hydrogen ESD process. The constant ion current for $m/z = 2$ (H_2^+) during the electron beam exposure suggests that the hydrogen ESD process is not depleting the hydrogen coverage as implied by the stepwise sequence of surface reactions shown in Figure 1. GaN growth must be occurring by alternative mechanisms at close to full hydrogen coverage. One possible alternative mechanism is illustrated in Figure 13. In this growth mechanism, the adsorption of TMG and NH_3 occurs primarily through Lewis acid-Lewis base interactions. The hydrogen ESD facilitates Ga-N bond formation from species in the initial Lewis acid-Lewis base complex. Additional experiments will be required to unravel the complexity of the electron-enhanced film growth at low temperatures.

3.7. Electron Enhancement for Other Thin Films and Competing Growth and Etching. This work has demonstrated that electron enhancement via hydrogen ESD can be used to grow crystalline GaN films at room temperature and 100 °C. Hydrogen ESD can occur from other materials such as

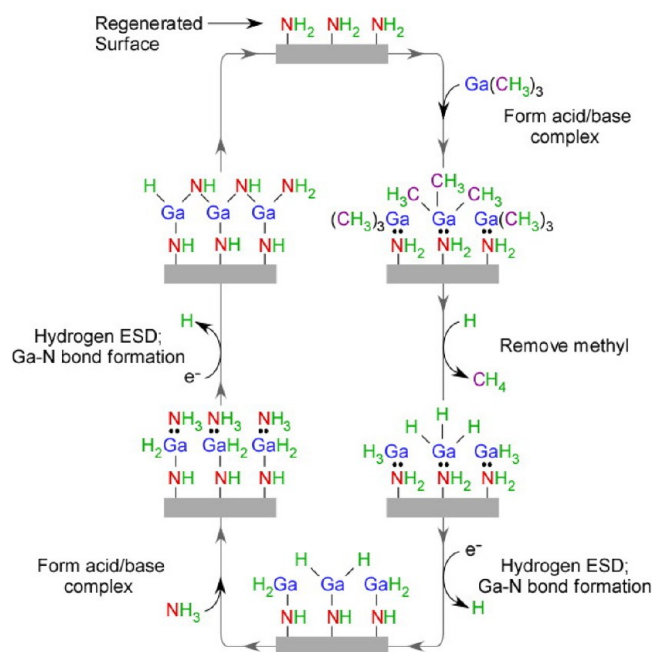


Figure 13. Alternative growth mechanism for electron-enhanced GaN growth using sequential surface reactions.

silicon,^{26–30} diamond⁷¹ and TiO_2 .⁷² Hydrogen ESD could facilitate the low temperature growth of these materials. Other surface species, such as halogens, could also be desorbed to induce low temperature film growth.⁷³ Consequently, this electron enhanced growth technique could facilitate the low temperature deposition of a wide range of other materials. Future possibilities include the electron enhanced growth of: silicon with Si_2H_6 ; SiC with Si_2H_6 and $CH_2=CH_2$; and diamond with $CH_2=CH_2$.

The competing etching during ESD revealed by the mass spectrometer measurements is an associated electron-induced process. This competing etching process may also be beneficial. Material that is not part of a crystalline lattice may be more favorably etched by the electron beam. The electrons would then both lead to film growth and also provide a means to remove amorphous material. The competing growth and etching processes may be required to obtain the crystalline GaN films at low temperatures. A similar competing process between growth and etching has been proposed to explain the smoothing of diamond films during diamond CVD.^{74,75}

4. CONCLUSIONS

The growth of crystalline GaN thin films at low temperatures was demonstrated using low energy electrons at 50 eV. Electrons are able to desorb hydrogen from the GaN surface and produce dangling bonds that facilitate Ga-N bond formation. GaN films were deposited over areas >5 cm² at room temperature and 100 °C on Si(111) wafers. The GaN growth procedure was a cycle of reactions similar to the reaction sequences employed for GaN ALD. TMG, H radicals and NH_3 were employed as the reactants. The electrons were included in the reaction cycle after the TMG/H and NH_3 exposures.

The GaN films grew linearly with the number of reaction cycles. The GaN film thicknesses were correlated with the electron flux and the GaN films were thicker closer to the electron gun. Linear growth rates from 0.9 to 1.3 Å/cycle were

measured depending on the electron flux. GIXRD analysis of the GaN films was consistent with polycrystalline films in the wurtzite crystal structure. TEM images also showed crystalline grains with diameters between 2 and 10 nm depending on temperature. The GaN films that were capped with Al contained no oxygen. However, the carbon concentration in the GaN films was between 10 and 35 at. %. The carbon concentration may have resulted from TMG pyrolysis on the hot surfaces of the hydrogen atom beam source (HABS) that produces CH₃ radicals.

The pressure of H₂ and various GaN etch products increased during the electron beam exposures during the reaction cycles. The constant ion currents for the H₂ and gallium hydride etch products during the electron beam exposures suggested that the reduction in hydrogen coverage resulting from hydrogen ESD is negligible. Alternatively, hydrogen rapidly refills the dangling bond sites from hydrogen reservoirs. The ion currents corresponding to the H₂ and GaN etch products increased with electron beam energy from 25 to 200 eV. These mass spectrometry results indicate that the electron enhanced GaN growth occurs concurrently with competing GaN etching. The competing etching may be able to remove amorphous GaN and produce crystalline GaN at low temperatures. The ability of ESD to remove hydrogen or other surface species may facilitate the low temperature growth of a wide range of materials.

AUTHOR INFORMATION

Notes

The authors declare no competing financial interest.

ACKNOWLEDGMENTS

This work was supported by Defense Advanced Research Projects Agency (DARPA) under grant W911NF-13-1-0041. The authors thank Brian Holloway, Tyler McQuade, and Anne Fischer from DARPA for their support and helpful comments. The authors also are grateful to John Russell and Chip Eddy from the Naval Research Laboratory for useful discussions and for providing the single-crystal GaN wafer. The authors also thank Andres Jaramillo-Botero and William Goddard from the California Institute of Technology for many useful suggestions. In addition, the authors acknowledge Kenneth Smith and Donald David from the University of Colorado Integrated Instrument Development Facility for their help with system design, development, and computer interfacing.

REFERENCES

- (1) Denbaars, S. P. Gallium Nitride Based Materials for Blue to Ultraviolet Optoelectronics Devices. *Proc. IEEE* **1997**, *85*, 1740–1749.
- (2) Zhu, D.; Wallis, D. J.; Humphreys, C. J. Prospects of III-Nitride Optoelectronics Grown on Si. *Rep. Prog. Phys.* **2013**, *76*, 106501.
- (3) Mishra, U. K.; Shen, L.; Kazior, T. E.; Wu, Y.-F. GaN-Based RF Power Devices and Amplifiers. *Proc. IEEE* **2008**, *96*, 287–305.
- (4) Pearton, S. J.; Ren, F. GaN Electronics. *Adv. Mater.* **2000**, *12*, 1571–1580.
- (5) Denis, A.; Goglio, G.; Demazeau, G. Gallium Nitride Bulk Crystal Growth Processes: A Review. *Mater. Sci. Eng., R* **2006**, *50*, 167–194.
- (6) Gibart, P. Metal Organic Vapour Phase Epitaxy of GaN and Lateral Overgrowth. *Rep. Prog. Phys.* **2004**, *67*, 667–715.
- (7) Khan, M. A.; Kuznia, J. N.; Vanhove, J. M.; Olson, D. T.; Krishnankutty, S.; Kolbas, R. M. Growth of High Optical and Electrical Quality GaN Layers Using Low Pressure Metalorganic Chemical Vapor Deposition. *Appl. Phys. Lett.* **1991**, *58*, 526–527.
- (8) Neumayer, D. A.; Ekerdt, J. G. Growth of Group III Nitrides. A Review of Precursors and Techniques. *Chem. Mater.* **1996**, *8*, 9–25.

(9) Molnar, R. J.; Moustakas, T. D. Growth of Gallium Nitride by Electron Cyclotron Resonance Plasma-Assisted Molecular Beam Epitaxy - The Role of Charged Species. *J. Appl. Phys.* **1994**, *76*, 4587–4595.

(10) Lei, T.; Moustakas, T. D.; Graham, R. J.; He, Y.; Berkowitz, S. J. Epitaxial Growth and Characterization of Zincblende Gallium Nitride on (001) Silicon. *J. Appl. Phys.* **1992**, *71*, 4933–4943.

(11) George, S. M. Atomic Layer Deposition: An Overview. *Chem. Rev.* **2010**, *110*, 111–131.

(12) Huang, S. C.; Wang, H. Y.; Hsu, C. J.; Gong, J. R.; Chiang, C. I.; Tu, S. L.; Chang, H. Growth of Wurtzite GaN on (001)GaAs Substrates at Low Temperature by Atomic Layer Epitaxy. *J. Mater. Sci. Lett.* **1998**, *17*, 1281–1285.

(13) Karam, N. H.; Parodos, T.; Colter, P.; McNulty, D.; Rowland, W.; Schetzina, J.; Elmasry, N.; Bedair, S. M. Growth of Device-Quality GaN at 550 Degrees C by Atomic Layer Epitaxy. *Appl. Phys. Lett.* **1995**, *67*, 94–96.

(14) Khan, M. A.; Skogman, R. A.; Vanhove, J. M.; Olson, D. T.; Kuznia, J. N. Atomic Layer Epitaxy of GaN over Sapphire Using Switched Metalorganic Chemical Vapor Deposition. *Appl. Phys. Lett.* **1992**, *60*, 1366–1368.

(15) Sumakeris, J.; Sitar, Z.; Aileytrent, K. S.; More, K. L.; Davis, R. F. Layer-by-Layer Epitaxial Growth of GaN at Low Temperatures. *Thin Solid Films* **1993**, *225*, 244–249.

(16) Koukitsu, A.; Kumagai, Y.; Taki, T.; Seki, H. Halogen Transport Atomic Layer Epitaxy of Cubic GaN Monitored by in situ Gravimetric Method. *Jpn. J. Appl. Phys., Part 1* **1999**, *38*, 4980–4982.

(17) Kumagai, Y.; Mayumi, M.; Koukitsu, A.; Seki, H. In situ Gravimetric Monitoring of Halogen Transport Atomic Layer Epitaxy of Cubic GaN. *Appl. Surf. Sci.* **2000**, *159–160*, 427–431.

(18) Kim, O. H.; Kim, D.; Anderson, T. Atomic Layer Deposition of GaN Using GaCl₃ and NH₃. *J. Vac. Sci. Technol., A* **2009**, *27*, 923–928.

(19) Tsuchiya, H.; Akamatsu, M.; Ishida, M.; Hasegawa, F. Layer-by-Layer growth of GaN on GaAs Substrates by Alternate Supply of GaCl₃ and NH₃. *Jpn. J. Appl. Phys., Part 2* **1996**, *35*, L748–L750.

(20) Ozgit, C.; Donmez, I.; Alevli, M.; Biyikli, N. Atomic Layer Deposition of GaN at Low Temperatures. *J. Vac. Sci. Technol., A* **2012**, *30*, 01A124.

(21) Ozgit-Akgun, C.; Goldenberg, E.; Okyay, A. K.; Biyikli, N. Hollow Cathode Plasma-Assisted Atomic Layer Deposition of Crystalline AlN, GaN and Al_xGa_{1-x}N Thin Films at Low Temperatures. *J. Mater. Chem. C* **2014**, *2*, 2123–2136.

(22) Madey, T. E.; Yates, J. T. Electron Stimulated Desorption as a Tool for Studies of Chemisorption - Review. *J. Vac. Sci. Technol.* **1971**, *8*, 525–555.

(23) Ramsier, R. D.; Yates, J. T. Electron Stimulated Desorption - Principles and Applications. *Surf. Sci. Rep.* **1991**, *12*, 246–378.

(24) Bellitto, V. J.; Thoms, B. D.; Koleske, D. D.; Wickenden, A. E.; Henry, R. L. Efficient Electron Stimulated Desorption of Hydrogen from GaN(0001). *Phys. Rev. B: Condens. Matter Mater. Phys.* **1999**, *60*, 4821–4825.

(25) Bermudez, V. M.; Koleske, D. D.; Wickenden, A. E. The Dependence of the Structure and Electronic Properties of Wurtzite GaN Surfaces on the Method of Preparation. *Appl. Surf. Sci.* **1998**, *126*, 69–82.

(26) Adams, D. P.; Mayer, T. M.; Swartzentruber, B. S. Nanometer-Scale Lithography on Si(001) Using Adsorbed H as an Atomic Layer Resist. *J. Vac. Sci. Technol., B: Microelectron. Process. Phenom.* **1996**, *14*, 1642–1649.

(27) Albert, M. M.; Tolk, N. H. Absolute Total Cross Sections for Electron Stimulated Desorption of Hydrogen and Deuterium from Silicon(111) Measured by Second Harmonic Generation. *Phys. Rev. B: Condens. Matter Mater. Phys.* **2001**, *63*, 035308.

(28) Avouris, P.; Walkup, R. E.; Rossi, A. R.; Akpati, H. C.; Nordlander, P.; Shen, T. C.; Abeln, G. C.; Lyding, J. W. Breaking Individual Chemical Bonds via STM-Induced Excitations. *Surf. Sci.* **1996**, *363*, 368–377.

(29) Fuse, T.; Fujino, T.; Ryu, J. T.; Katayama, M.; Oura, K. Electron Stimulated Desorption of Hydrogen from H/Si(001)-1 × 1 Surface

Studied by Time-of-Flight Elastic Recoil Detection Analysis. *Surf. Sci.* **1999**, *420*, 81–86.

(30) Shen, T. C.; Wang, C.; Abeln, G. C.; Tucker, J. R.; Lyding, J. W.; Avouris, P.; Walkup, R. E. Atomic-Scale Desorption Through Electronic and Vibrational Excitation Mechanisms. *Science* **1995**, *268*, 1590–1592.

(31) Menzel, D.; Gomer, R. Desorption from Metal Surfaces by Low Energy Electrons. *J. Chem. Phys.* **1964**, *41*, 3311–3328.

(32) Redhead, P. A. Interaction of Slow Electrons with Chemisorbed Oxygen. *Can. J. Phys.* **1964**, *42*, 886–905.

(33) Feibelman, P. J.; Knotek, M. L. Reinterpretation of Electron Stimulated Desorption Data from Chemisorption Systems. *Phys. Rev. B: Condens. Matter Mater. Phys.* **1978**, *18*, 6531–6539.

(34) Knotek, M. L.; Feibelman, P. J. Ion Desorption by Core-Hole Decay. *Phys. Rev. Lett.* **1978**, *40*, 964–967.

(35) Bellitto, V. J.; Yang, Y.; Thoms, B. D.; Koleske, D. D.; Wickenden, A. E.; Henry, R. L. Desorption of Hydrogen from GaN(0001) Observed by HREELS and ELS. *Surf. Sci.* **1999**, *442*, L1019–L1023.

(36) Chiang, C. M.; Gates, S. M.; Bensaoula, A.; Schultz, J. A. Hydrogen Desorption and Ammonia Adsorption on Polycrystalline GaN Surfaces. *Chem. Phys. Lett.* **1995**, *246*, 275–278.

(37) Shekhar, R.; Jensen, K. F. Temperature Programmed Desorption Investigations of Hydrogen and Ammonia Reactions on GaN. *Surf. Sci.* **1997**, *381*, L581–L588.

(38) Lyding, J. W.; Shen, T. C.; Hubacek, J. S.; Tucker, J. R.; Abeln, G. C. Nanoscale Patterning and Oxidation of H-Passivated Si(100)2 × 1 Surfaces with an Ultrahigh Vacuum Scanning Tunneling Microscope. *Appl. Phys. Lett.* **1994**, *64*, 2010–2012.

(39) Becker, R. S.; Higashi, G. S.; Chabal, Y. J.; Becker, A. J. Atomic Scale Conversion of Clean Si(111)-H-1 × 1 to Si(111)-2 × 1 by Electron Stimulated Desorption. *Phys. Rev. Lett.* **1990**, *65*, 1917–1920.

(40) Hitosugi, T.; Hashizume, T.; Heike, S.; Watanabe, S.; Wada, Y.; Hasegawa, T.; Kitazawa, K. Scanning Tunneling Spectroscopy of Dangling-Bond Wires Fabricated on the Si(100)-2 × 1-H Surface. *Jpn. J. Appl. Phys., Part 2* **1997**, *36*, L361–L364.

(41) Shen, T. C.; Wang, C.; Lyding, J. W.; Tucker, J. R. Nanoscale Oxide Patterns on Si(100) Surfaces. *Appl. Phys. Lett.* **1995**, *66*, 976–978.

(42) Shen, T. C.; Wang, C.; Tucker, J. R. Al Nucleation on Monohydride and Bare Si(001) Surfaces: Atomic Scale Patterning. *Phys. Rev. Lett.* **1997**, *78*, 1271–1274.

(43) Randall, J. N.; Lyding, J. W.; Schmucker, S.; Von Ehr, J. R.; Ballard, J.; Saini, R.; Xu, H.; Ding, Y. Atomic Precision Lithography on Si. *J. Vac. Sci. Technol. B* **2009**, *27*, 2764–2768.

(44) Koebley, S. R.; Outlaw, R. A.; Dellwo, R. R. Degassing a Vacuum System with in situ UV Radiation. *J. Vac. Sci. Technol., A* **2012**, *30*, 060601.

(45) Bermudez, V. M. Theoretical Study of Hydrogen Adsorption on the GaN(0001) Surface. *Surf. Sci.* **2004**, *565*, 89–102.

(46) Nepal, N.; Qadri, S. B.; Hite, J. K.; Mahadik, N. A.; Mastro, M. A.; Eddy, C. R., Jr. Epitaxial Growth of AlN Films via Plasma-Assisted Atomic Layer Epitaxy. *Appl. Phys. Lett.* **2013**, *103*, 082110.

(47) Langford, J. I.; Wilson, A. J. C. Scherrer After 60 Years - Survey and Some New Results in Determination of Crystallite Size. *J. Appl. Crystallogr.* **1978**, *11*, 102–113.

(48) Commercial equipment, instruments, or materials are identified only in order to adequately specify certain procedures. In no case does such identification imply recommendation or endorsement by the National Institute of Standards and Technology, nor does it imply that the products identified are necessarily the best available for the purpose.

(49) Cobine, J. D. *Gaseous Conductors: Theory and Engineering Applications*; McGraw-Hill Book Company, Inc.: New York, 1941.

(50) Ejder, E. Refractive Index of GaN. *Phys. Status Solidi A - Applied Research* **1971**, *6*, 445–448.

(51) Joint Committee on Powder Diffraction Standards (JCPDS). *JCPDS File 88-2361*.

(52) Balkas, C. M.; Davis, R. F. Synthesis Routes and Characterization of High-Purity, Single-Phase Gallium Nitride Powders. *J. Am. Ceram. Soc.* **1996**, *79*, 2309–2312.

(53) Kumar, M. S.; Kumar, J. XRD, XPS, SEM, PL and Raman Scattering Analysis of Synthesised GaN Powder. *Mater. Chem. Phys.* **2003**, *77*, 341–345.

(54) Ishibashi, A.; Takeishi, H.; Mannoh, M.; Yabuuchi, Y.; Ban, Y. Residual Impurities in GaN/Al₂O₃ Grown by Metalorganic Vapor Phase Epitaxy. *J. Electron. Mater.* **1996**, *25*, 799–803.

(55) Chen, Q.; Dapkus, P. D. On the Thermal Decomposition of Trimethylgallium - A Molecular Beam Sampling Mass Spectroscopy Study. *J. Electrochem. Soc.* **1991**, *138*, 2821–2826.

(56) Francis, J. T.; Benson, S. W.; Tsotsis, T. T. Observation of the Methyl Radical During the Surface Decomposition Reaction of Trimethylgallium. *J. Phys. Chem.* **1991**, *95*, 4583–4586.

(57) Lam, H. T.; Vohs, J. M. Surface Reactions of Trimethylgallium on MOVPE-Grown GaN(0001). *Surf. Sci.* **1999**, *426*, 199–211.

(58) Armitage, R.; Hong, W.; Yang, Q.; Feick, H.; Gebauer, J.; Weber, E. R.; Hautakangas, S.; Saarinen, K. Contributions from Gallium Vacancies and Carbon-Related Defects to the “Yellow Luminescence” in GaN. *Appl. Phys. Lett.* **2003**, *82*, 3457–3459.

(59) DeMierry, P.; Ambacher, O.; Kratzer, H.; Stutzmann, M. Yellow Luminescence and Hydrocarbon Contamination in MOVPE-Grown GaN. *Phys. Status Solidi A - Applied Research* **1996**, *158*, 587–597.

(60) Wright, A. F. Substitutional and Interstitial Carbon in Wurtzite GaN. *J. Appl. Phys.* **2002**, *92*, 2575–2585.

(61) Gillis, H. P.; Choutov, D. A.; Martin, K. P.; Pearton, S. J.; Abernathy, C. R. Low Energy Electron-Enhanced Etching of GaN/Si in Hydrogen Direct Current Plasma. *J. Electrochem. Soc.* **1996**, *143*, L251–L253.

(62) Madden, H. H.; Jennison, D. R.; Traum, M. M.; Margaritondo, G.; Stoffel, N. G. Correlation of Stimulated H⁺ Desorption Threshold with Localized State Observed in Auger Line Shape - Si(100)-H. *Phys. Rev. B: Condens. Matter Mater. Phys.* **1982**, *26*, 896–902.

(63) Pian, T. R.; Tolk, N. H.; Traum, M. M.; Kraus, J.; Collins, W. E. Energy Dependence of Electron Stimulated Desorption of Excited Neutral Alkalis from Alkali Halides. *Surf. Sci.* **1983**, *129*, 573–580.

(64) Nakatsuji, K.; Matsuda, K.; Yonezawa, T.; Daimon, H.; Suga, S. Adsorption and Desorption Processes of Cl on a Si(100) Surface. *Surf. Sci.* **1996**, *363*, 321–325.

(65) Stawinski, U.; Bauer, E. Alkali Halide Layers on W(110) - Electron Stimulated Desorption of Ions, Structure, and Composition. *Phys. Rev. B: Condens. Matter Mater. Phys.* **1993**, *47*, 12820–12831.

(66) Pearton, S. J.; Abernathy, C. R.; Vartuli, C. B.; Lee, J. W.; MacKenzie, J. D.; Wilson, R. G.; Shul, R. J.; Ren, F.; Zavada, J. M. Unintentional Hydrogenation of GaN and Related Alloys During Processing. *J. Vac. Sci. Technol. A* **1996**, *14*, 831–835.

(67) Zavada, J. M.; Wilson, R. G.; Abernathy, C. R.; Pearton, S. J. Hydrogenation of GaN, AlN and InN. *Appl. Phys. Lett.* **1994**, *64*, 2724–2726.

(68) George, S. M.; Desantolo, A. M.; Hall, R. B. Surface Diffusion of Hydrogen on Ni(100) Studied Using Laser Induced Thermal Desorption. *Surf. Sci.* **1985**, *159*, L425–L432.

(69) Mak, C. H.; Brand, J. L.; Deckert, A. A.; George, S. M. Surface Diffusion of Hydrogen on Ru(001) Studied Using Laser Induced Thermal Desorption. *J. Chem. Phys.* **1986**, *85*, 1676–1680.

(70) Schafer, J.; Simons, A.; Wolfrum, J.; Fischer, R. A. Detection of Gas-Phase Species in MOCVD of GaN Using Molecular Beam Quadrupole Mass Spectrometry. *Chem. Phys. Lett.* **2000**, *319*, 477–481.

(71) Goeden, C.; Dollinger, G. Electron Stimulated Hydrogen Desorption from Diamond Surfaces and its Influence on the Low Pressure Synthesis of Diamond. *Appl. Phys. Lett.* **2002**, *81*, S027–S029.

(72) Suzuki, S.; Fukui, K.; Onishi, H.; Iwasawa, Y. Hydrogen Adatoms on TiO₂(110)-(1 × 1) Characterized by Scanning Tunneling Microscopy and Electron Stimulated Desorption. *Phys. Rev. Lett.* **2000**, *84*, 2156–2159.

(73) Trenhaile, B. R.; Antonov, V. N.; Xu, G. J.; Agrawal, A.; Signor, A. W.; Butera, R. E.; Nakayama, K. S.; Weaver, J. H. Phonon-Activated

Electron Stimulated Desorption of Halogens from Si(100)-(2 × 1). *Phys. Rev. B: Condens. Matter Mater. Phys.* **2006**, *73*, 125318.

(74) Battaile, C. C.; Srolovitz, D. J.; Oleinik, II; Pettifor, D. G.; Sutton, A. P.; Harris, S. J.; Butler, J. E. Etching Effects During the Chemical Vapor Deposition of (100) Diamond. *J. Chem. Phys.* **1999**, *111*, 4291–4299.

(75) Ivanov, O. A.; Muchnikov, A. B.; Chernov, V. V.; Bogdanov, S. A.; Vikharev, A. L.; Butler, J. E. Experimental Study of Hydrogen Plasma Etching of (100) Single Crystal Diamond in a MPACVD Reactor. *Mater. Lett.* **2015**, *151*, 115–118.